

Reproduction of cosmic dust analogues by non-equilibrium condensation in triple DC thermal plasma jet system

T. H. Kim¹, J. H. Oh², M. Kim², Y. H. Lee², S. H. Hong² and S. Choi^{1,2}

¹*Institute of Nuclear Science and Technology, Jeju National University, Jeju 64243, Republic of Korea*

²*Department of Nuclear and Energy Engineering, Jeju National University, Jeju 64243, Republic of Korea*

Abstract: Triple DC thermal plasma jet was applied for understanding of the formation process and environment of cosmic dust. Iron embedded amorphous silicate nanoparticles, which are very similar to amorphous silicates in cometary dust, were successfully reproduced in this work. The structural morphology of cosmic dust analogues was varied according to the quenching rate by plasma forming gas composition and residence time at the plasma flame.

Keywords: Cosmic dust, reproduction, synthesis, thermal plasma, condensation, non-equilibrium condensation

1. Introduction

Amorphous silicate is the major component of cosmic dust. It is considered to be one of the most primitive materials in the solar system. Chondritic porous interplanetary dust particles (CP IDPs) contain abundant amorphous silicate grains under 100 nm with Fe-Ni and FeS nanoparticles. It is known as GEMS (glass with embedded metal and sulfides). Two different origins of GEMS have been proposed; non-equilibrium condensation in the early solar nebula and amorphization by irradiation in interstellar medium [1,2]. However, they are still in controversy. Therefore, experimental study on non-equilibrium condensation of cosmic dust analogues as GEMS-like materials is crucial for determination of the GEMS and the solar system' origin.

In previous studies, nanoparticles with very similar structures to GEMS were formed using the ITP (Induction thermal plasma) system at 30 and 6 kW in a limited parameter range [3-5]. It was suggested that a high quenching rate is a key environment to reproduce GEMS-like textures. Subsequently, we performed condensation experiments with the single DC non-transferred thermal plasma jet to improve the quenching rate and offer higher temperature. Generally, the highest temperature of the thermal plasma jet discharged by DC non-transferred torch is typically higher (~15,000 K) than that of ITP (~10,000 K). Moreover, the quenching rate of thermal plasma is typically more than 10 times higher compared with ITP flame, since the plasma volume is smaller and flow velocity is rapider than ITP. However, the starting material was not sufficiently vaporized and GEMS-like material was not successfully synthesized. In the general singular thermal plasma jet system, it is difficult to penetrate the starting material into the prevalent high temperature of jet core, because the viscosity of plasma jet core is extremely high with highest velocity. Therefore, the starting material could not pass the relatively low temperature of jet rim, refractory starting material such as MgO is cooled from melts, not vapour. In our system, on the other hand, the

triple thermal plasma jets generated from the three torches are merged into the expanded long flame. The starting material injected between torches directly goes through the wider high temperature region.

In order to improve the vaporization and provide higher quenching rates, we carried out the vaporization and condensation experiments in the triple thermal plasma jet system. The equal starting material was used with those of previous experiments in ITP system [3-5]. A mixture of micron-sized metal and oxides powder was used as a starting material; Si, SiO₂, MgO, Fe, Na₂SiO₃, CaO, and Ni under 10 μm. The chemical composition having the averaged composition of GEMS [1] without sulfur was adopted as a starting material. In this study, the thermal plasma was discharged by an input power of 27 kW, which is higher than the previous ITP experiments at 6 kW to improve vaporization efficiency of the starting material. And the plasma forming gas was controlled by N₂ and H₂ to compare according to the quenching rate.

2. Experiments

A picture of triple DC thermal plasma jet system is indicated in Fig. 1(a). The system consists of a power supply, a plasma torch, a powder feeder for the injection of the starting materials. The starting material was injected into the merged plasma flame from the nozzle which is located between three torches in Fig. 1(b). A reactor is separated into seven numbering parts and cyclone filter. The produced powder was collected at the inner wall in each numbered reactor. All side of the reactor is cooled by running water. The three plasma jets were generated at individual torches in Fig. 1(c), and they were merged into an expanded flame in Fig. 1(d).

Detail of experimental conditions was described in Table 1. The experiments were carried out according to the plasma forming gas composition; (1) Ar-N₂ plasma and (2)

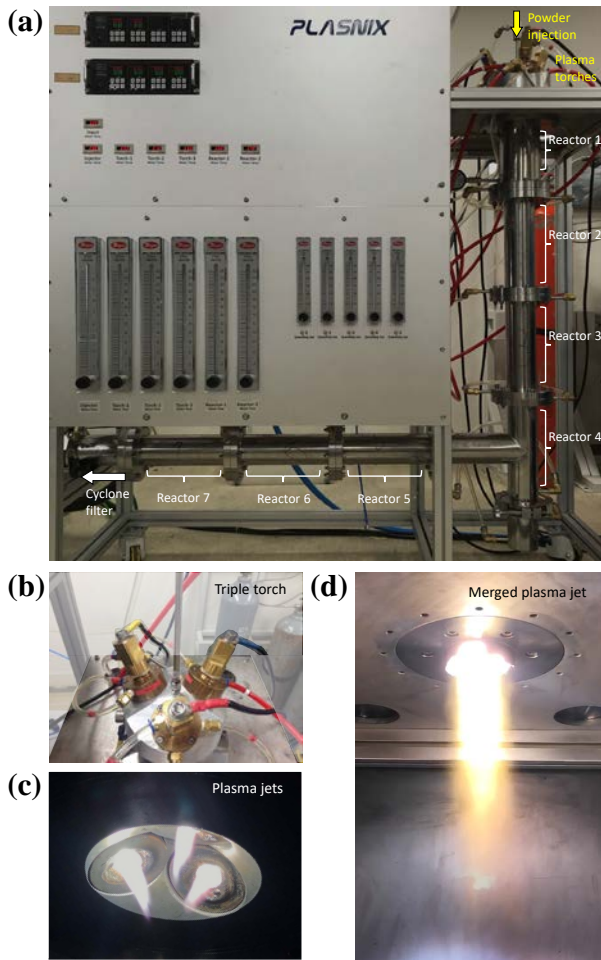


Fig. 1. Picture of (a) triple DC thermal plasma jet system and (b) top view of torch fabrication. (c) Generated triple plasma jet and (d) a merged plasma flame.

Ar-H₂ plasma. Input power of each torch was 9 kW, therefore, total input power from three torches was applied at about 27 kW. The reactor pressure was maintained at atmospheric pressure. The flow rate of plasma forming gas was 14 L/min Ar with 14 L/min N₂ or H₂. The starting

Table 1. X-ray diffraction patterns of (a) starting material and (b) synthesized powder by Ar-N₂ and Ar-H₂ thermal plasma.

	Ar-N ₂ plasma	Ar-H ₂ plasma
Total input power	About 27 kW	
Plasma forming gas	14 L/min Ar, 14 L/min N ₂	14 L/min Ar, 14 L/min H ₂
Chamber pressure	1 atm	
Starting materials	Si-Mg-Fe-Na-Al-Ca-Ni-O system Mixture of powders (~10 μm) (Si, SiO ₂ , MgO, Fe, Na ₂ SiO ₃ , CaO, Ni)	
Feeding rate	300 mg/min	
Carrier gas	5 L/min Ar	

material was used as systems of Si-Mg-Fe-Na-Al-Ca-Ni-O in this work. This starting material is same as in the previous experiments that were carried out in ref. [6]. It consists of micron-sized oxides and metallic powders (Si, SiO₂, MgO, Fe, Al₂O₃, CaO, Na₂SiO₃, and Ni powder reagents) as representative of the solar abundance [1]. Their average particle size was under 10 μm. The feeding rate of starting material was fixed at 300 mg/min, and Ar was used as carrier gas for injection.

The starting materials and produced condensates were analyzed with X-ray diffraction (XRD, DMAX 2500, Rigaku) using CuKα radiation and observed with transmission electron microscope (TEM, JEM-2100F, JEOL).

3. Results and discussion

Fig. 2 shows XRD patterns of the starting material and products according to the plasma forming gas. In the XRD pattern of the starting material, most of individual components were detected except for Al₂O₃ and Na₂SiO₃, because of their small amounts. The XRD pattern of run products have sharp peaks of metallic iron, iron nickel, and iron silicide. It means that the amorphous materials including Si, Mg, Na, Ca, Ni, and O were synthesized from the starting material. Although the intensity of peaks is universally weak, the synthesized those of FeNi and Fe₃Si

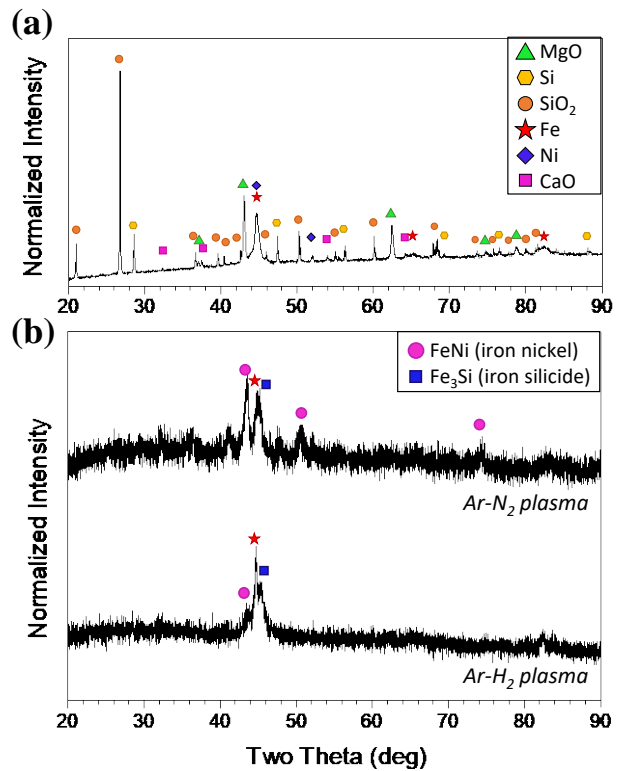
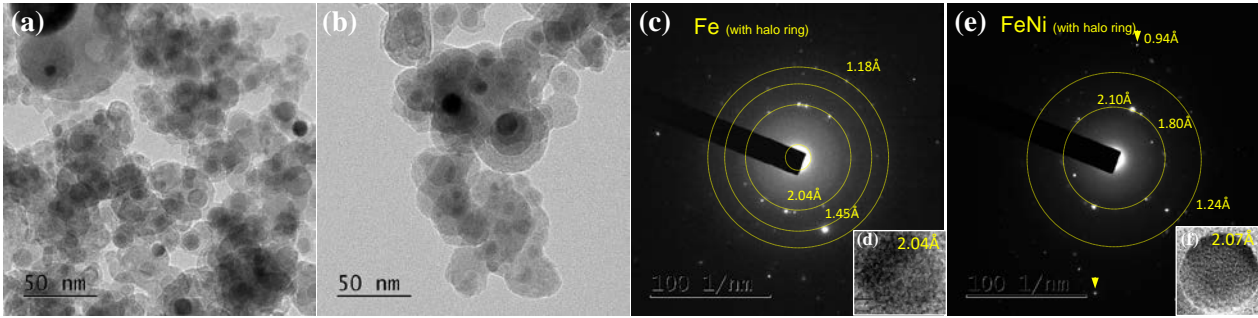


Fig. 2. X-ray diffraction patterns of (a) starting material and (b) synthesized products by Ar-N₂ and Ar-H₂ thermal plasma.

Ar-N₂ plasma



Ar-H₂ plasma

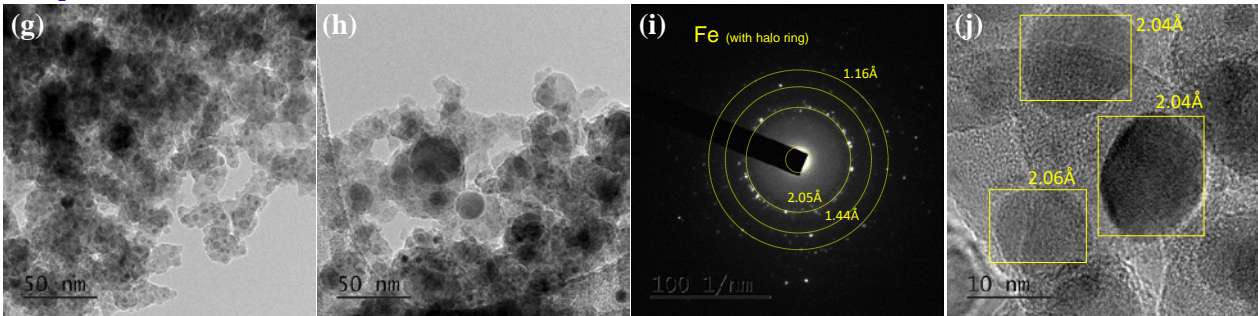


Fig. 3. FE-TEM images of synthesized cosmic dust analogues by (a,b) Ar-N₂ and (g,h) Ar-H₂ plasma. SAED patterns of core embedded area in nanomaterial in (c,e) Ar-N₂ and (i) Ar-H₂ plasma conditions. HR-images of embedded nanoparticles inside amorphous material in (d,f) Ar-N₂ and (j) Ar-H₂ plasma conditions.

are relatively weaker in Ar-H₂ plasma condition compared with Ar-N₂ plasma condition.

Images of FE-TEM, HR-TEM, SAED patterns are indicated according to the plasma forming gas composition in Fig. 3. Upper and lower part are for Ar-N₂ and Ar-H₂ plasma condition, respectively. The spherical nanoparticles inside the non-specific shaped material were observed in both conditions. The size of nanoparticles is smaller and denser in Ar-H₂ plasma condition. The average particle size of embedded material is under 10 nm in Fig. 3 (g), in spite of about 20 nm in Fig. 3(a). In Fig. 3(c)-(f), the embedded spheres were analysed as Fe or FeNi. Only Fe nanoparticles were embedded in the synthesized nanomaterial in Fig. 3(i) and (j) of Ar-H₂ plasma condition. It was supposed that the largest difference between Ar-N₂ and Ar-H₂ plasma environment is quenching rate variation by different temperature distribution and reduction environment by hydrogen gas, and the embedded particles might be condensed more rapidly in Ar-H₂ plasma condition. In order to investigate in details, analytical result of chemical composition will be discussed in the presentation.

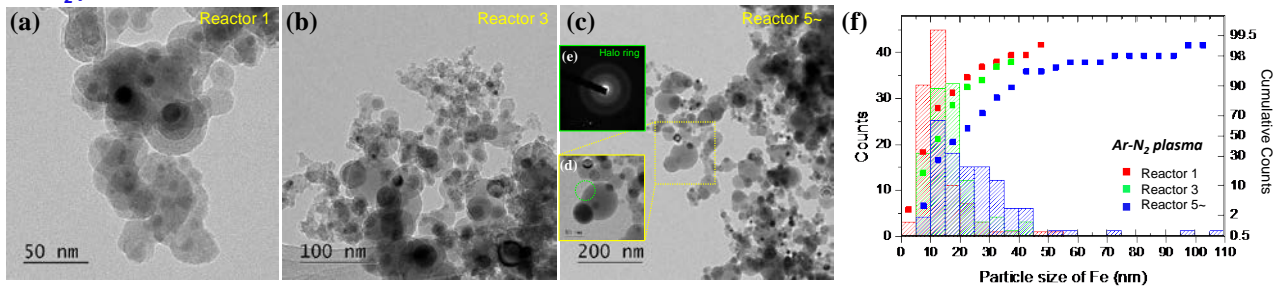
Fig. 4 shows the morphology and structural characteristic of synthesized nanomaterials according to the collected part. In both condition of Ar-N₂ and Ar-H₂, the particle size of embedded metals is increased according to the Reactor number. In addition, the metallic nanoparticles are moved into the outer side of amorphous nanomaterials. We suppose that the embedded nanoparticles are merged and larger by late condensation

at the backward reactor. The merged plasma jet was expanded into longer plasma flame over Reactor 1 and 2. It means that the product collected at the forward reactor should be quickly condensed compared with backward reactor. Therefore, product condensed in backward reactor had longer residence time to grow in the high temperature region. And then, the merged nanoparticle core moved to outer layer of body material. It was confirmed that the amorphous layer was observed outside of metallic nanoparticles in Fig. 4(c) and (i). The size of embedded nanoparticles increased according to the reactor number Fig. 4(f) and (k). Furthermore, the average particle size in each reactor was smaller in Ar-H₂ plasma condition than Ar-N₂ plasma condition. It supported the estimation we discussed in Fig. 3. We will discuss in minute detail about the formation process and influence of quenching rate by plasma forming gas composition in the presentation.

4. Summary and future plan

We successfully reproduced the cosmic dust analogues as improving the previous experiments by DC non-transferred thermal plasma and ITP systems. From the previous experiments, it was revealed that the rapid quenching is key condition and parameter to create non-equilibrium condensation environment and produce metal embedded amorphous silicates as cometary GEMS. In this study, the quenching rate or residence time at the high temperature environment was controlled by plasma forming gas composition and collected position. The size

Ar-N₂ plasma



Ar-H₂ plasma

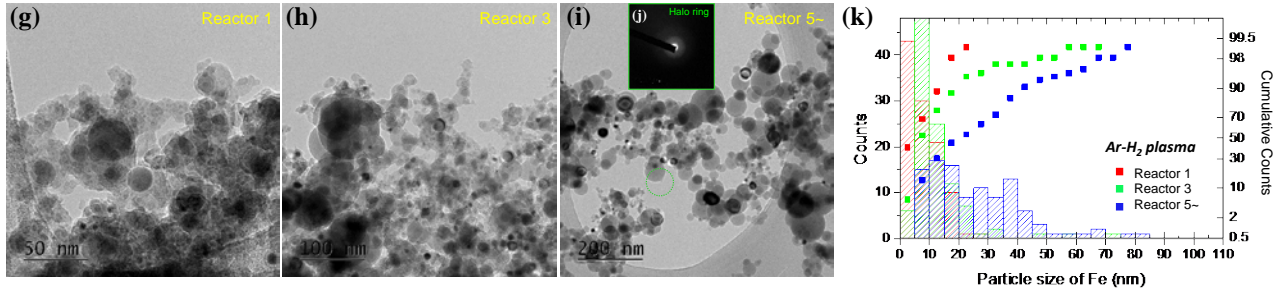


Fig. 4. FE-TEM images, SAED patterns, and particle size distribution of synthesized product according to the collected position in Ar-N₂ or Ar-H₂ plasma condition. (a) Reactor 1, (b) Reactor 3, (c,d,e) backward reactor in Ar-N₂ plasma condition. (g) Reactor 1, (h) Reactor 3, (i,j) backward reactor in Ar-H₂ plasma condition. Particle size distributions of embedded metallic nanoparticles in (f) Ar-N₂ or (k) Ar-H₂ plasma.

and density of embedded metallic nanoparticles have strong influence according to the plasma forming gas composition. Hydrogen gas reduced the nanoparticles' size and is able to be denser them. The texture of nanomaterial was affected by residence time in the high temperature region unable condensation. The embedded nanoparticles were merged and moved to outer layer of amorphous silicates by late quenching. The comparison of synthesized product will be presented and the formation process and critical environment will be suggested in this presentation.

5. References

- [1] L. P. Keller, S. Messenger, *Geochimica et Cosmochimica Acta*, 75, 5336-5365 (2011).
- [2] J. P. Bradley, Z. R. Dai, *Astrophys. J.*, 617, 650-655 (2004).
- [3] J. Matsuno (2015), Ph.D. thesis, Kyoto University, Japan.
- [4] M. Tanaka, J. Noda, T. Watanabe et al., *J. Phys.: conference series*, 518, 012025 (2014)
- [5] T. H. Kim, A. Tsuchiyama, A. Takigawa, J. Matsuno, *ISPC 23 (23rd International Symposium on Plasma Chemistry)*, P2-33-7 (2017). [3] T. H. Kim, S. Choi, D. W. Park, *J. Korean Phys. Soc.*, 63, 10, 1864-1870 (2013)